ChemPubSoc Europe

DOI: 10.1002/cphc.201700785

CHEMPHYSCHEM Communications

Special Issue

Influence of Levulinic Acid Hydrogenation on Aluminum Coordination in Zeolite-Supported Ruthenium Catalysts: A ^{27}Al 3QMAS Nuclear Magnetic Resonance Study**

Wenhao Luo,[a, b] Ernst R. H. van Eck,[c] Pieter C. A. Bruijnincx,*[a] and Bert M. Weckhuysen*[a]

The influence of a highly oxygenated, polar protic reaction medium, that is, levulinic acid in 2-ethylhexanoic acid, on the dealumination of two zeolite-supported ruthenium catalysts, namely Ru/H-β and Ru/H-ZSM-5, has been investigated by ^{27}Al triple-quantum magic-angle spinning nuclear magnetic resonance spectroscopy (3QMAS NMR). Upon use of these catalysts in the hydrogenation of levulinic acid, the heterogeneity in aluminum speciation is found to increase for both Ru/H-ZSM-5 and Ru/H-β. For Ru/H-ZSM-5, the symmetric, tetrahedral framework aluminum species (FAL) were found to be mainly converted into distorted tetrahedral FAL species, with limited loss of aluminum to the solution by leaching. A severe loss of both FAL and extra-framework aluminum (EFAL) species into the liquid phase was observed for Ru/H-β instead. The large decrease in tetrahedral FAL species, in particular, results in a significant decrease in strong acid sites, as corroborated by Fourier transform infrared spectroscopy (FT-IR). This decrease in acidity, evidence of the inferior stability of the strongly acidic sites in Ru/H-β relative to Ru/H-ZSM-5 under the applied conditions, is considered as the main reason for differences seen in catalyst performance.

The acidity of zeolites is known to strongly depend on the type of zeolite structure as well as on aluminum content and its distribution within the zeolite framework.[1,2] Hydrolytic removal of framework aluminum, that is, zeolite dealumination, results in modification of the number, nature (Brønsted acidic (BAS) vs. Lewis acidic sites (LAS)), strength, and location (framework vs. extra-framework) of the acid sites, ultimately altering the catalytic properties in various ways.[3–5] Subjecting zeolite-based materials to a medium of low pH and/or high polarity can, for instance, result in hydrolytic aluminum removal from their framework sites. The extent to which this removal takes place, is known to depend on zeolite structure, applied temperature and composition of the liquid phase. For example, framework dealumination of zeolite H-β has been reported using mineral acids, such as HCl,[6,7] as well as organic acids such as oxalic acid, which acts as both an acid and a chelating agent. Dealumination was found to be more severe for H-β than for H-ZSM-5 with this organic acid.[8]

While these examples were concerned with on-purpose dealumination to improve zeolite performance, such changes in aluminum content and—as a result—their acidity can also occur unintentionally if the zeolites are used as catalysts under demanding high temperature and pressure, liquid-phase conditions. Those harsh reaction conditions are typically used for the conversion of renewable biomass-derived substrates.[9–11] Some examples of zeolite-supported Ru catalyst subjected to polar conditions include the use of Ru on modified USY to convert cellulose into sugar alcohols,[12] Ru/H-Y and Ru-M/H-Y (with M = Fe, Ni, Cu and Zn) catalysts for the hydrodeoxygenation (HDO) of softwood lignin and its model compounds[13] and Ru/H-ZSM-5 for the HDO of lignin-derived phenolic monomers and dimers.[14]

Some zeolite-catalyzed, hydrothermal conversion processes of renewable substrates even involve the use of renewable organic acids, either as substrate, intermediate or as end product, providing an even harsher environment. In this sense, valorization of levulinic acid provides a particularly good example of both the great potential of zeolite(-supported) catalysts as well as the challenges involved. Levulinic acid (LA)[15–17] is a versatile platform molecule and can be converted, for example, into γ-valerolactone (GVL),[18,19] and pentanoic acid (PA) and its esters by sequential HDO steps.[20–22] Zeolites have been studied for the various acid-catalyzed steps involved in the sequence, again on occasion as part of bifunctional catalysts in combination with a metal hydrogenation function.[23,24] The Shell laboratory reported, for example, a H-β-based catalyst active for the conversion of ethyl levulinate into ethyl penta-

[a] Dr. W. Luo, Dr. P. C. A. Bruijnincx, Prof. Dr. B. M. Weckhuysen
Inorganic Chemistry and Catalysis
Debye Institute for Nanomaterials Science, Utrecht University
Universiteitsweg 99, 3584 CG
Utrecht (The Netherlands)
E-mail: p.c.a.bruijnincx@uu.nl
b.m.weckhuysen@uu.nl

[b] Dr. W. Luo
State Key Laboratory of Catalysis
Dalian Institute of Chemical Physics
Chinese Academy of Sciences, Zhongshan Road 457
Dalian 116023 (China)

[c] Dr. E. R. H. van Eck
Institute for Molecules and Materials
Radboud University, Heyendaalsweg 135
6525 AJ Nijmegen (The Netherlands)

[**] 3QMAS: Triple-Quantum Magic-Angle Spinning

Supporting Information and the ORCID identification number(s) for the author(s) of this article can be found under: https://doi.org/10.1002/cphc.201700785.

An invited contribution to a Special Issue on Reactions in Confined Spaces

noate,[25] and a Pt/H-ZSM-5-catalyzed process for the conversion of GVL into PA.[20] Limited information is available, however, on the stability of these zeolites and changes in aluminum content and speciation under these liquid phase processes. Further insight into such potential deactivation processes is therefore clearly needed.

We previously reported on Ru/H-β and Ru/H-ZSM-5 as catalyst materials capable of the direct HDO of LA into PA or its esters in dioxane.[21,22] It was found that the zeolite support material provided the strong acid sites essential for ring-opening of the reaction intermediate GVL. Changes in aluminum content and speciation were studied by FT-IR spectroscopy after pyridine adsorption to distinguish changes in LAS and BAS, while atom absorption spectroscopy (AAS) and one-dimensional (1D) magic angle spinning (MAS) ^{27}Al nuclear magnetic resonance (NMR) revealed leaching of Al and changes in the coordination of Al, respectively. These characterization studies showed that the highest loss of framework aluminum occurred for Ru/H-β after a 10 h reaction at 473 K in a solution of 2-ethylhexanoic acid (EHA). EHA was used as LA mimic to deliberately test the catalyst under a harsh environment of constant acid concentration. Preliminary studies on the changes in Al speciation by quantitative analysis of the 1D solid-state ^{27}Al NMR spectra showed that (1) more Al was lost to solution from H-β than from H-ZSM-5 and (2) the extent of leaching was different for four-, five- and six-coordinated Al species, with the latter leaching the most.[21]

To further assess the influence of the reaction environment on zeolite dealumination and—as a result—on the acidic properties of the catalysts, a detailed comparison of the aluminum speciation in the fresh and spent catalysts is required. While 1D ^{27}Al MAS NMR has been extensively applied to investigate the coordination state of Al (e.g. four (Al^{IV}) or six-coordinated Al (Al^{VI}) in zeolites),[26–29] such measurements also have their limitations. Indeed, each of the different coordination states may consist of different types of Al, which are often difficult to distinguish because of strongly overlapping signals in the low-resolution 1D MAS NMR spectra. Their lines are usually broadened by second-order quadrupolar effects, giving typical quadrupolar line shapes. In addition, structural disorder will further broaden and smear out the quadrupolar line shapes due to a distribution in both quadrupolar interaction as well as isotropic chemical shifts. Fortunately, two-dimensional (2D) ^{27}Al triple-quantum (3Q) MAS NMR may provide the enhanced resolution needed to study these zeolite materials in more detail. 3QMAS NMR provides 2D spectra where the anisotropic part of the quadrupolar interaction is separated from isotropic shift contributions.[30–32] Indeed, 3QMAS NMR is especially helpful for the analysis of 1D spectra of disordered materials.[33–38] The disorder can be reflected in the line shapes of the 3QMAS NMR spectra, and translated into interaction parameter distributions. In particular, ^{27}Al 3QMAS NMR has been successfully applied in structural studies of zeolites, allowing, for example, the differentiation and even quantification of the different Al species.[4,34,39,40] There has been an increasing interest in the quantification of this disorder recently[41–43] and a very valuable model was developed by Czjzek et al.,[44] able to describe the quadrupolar interaction parameter distribution resulting from the structural disorder.

Here, we report on the use of ^{27}Al 3QMAS NMR spectroscopy to differentiate between different Al species in fresh and spent Ru/H-β (Si/Al = 12.5, CP814E, Zeolyst) and Ru/H-ZSM-5 (Si/Al = 11.5, CBV2314, Zeolyst), including the determination of the related interaction parameter distributions. The obtained data have been fitted with the Czjzek model,[36,40,41] which quantitatively establishes the changes in the state of the various aluminum species. The insights obtained from advanced ^{27}Al 3QMAS NMR studies are compared with FT-IR spectroscopy data,[21] providing further insights into the changes in acidity (i.e., amount, nature, and location). Based on this knowledge a more detailed interpretation can be given of the differences in activity and deactivation behavior seen for both Ru/zeolite catalysts in the selective hydrogenation of LA to PA.

Catalytic performance of the Ru/H-ZSM-5 and Ru/H-β catalysts was assessed in the hydrogenation reaction of levulinic acid in EHA at 473 K and 40 bar H_2. After a reaction time of 10 h (Table S1), a two-fold higher PA yield was achieved with Ru/H-ZSM-5 (15.5%) compared to Ru/H-β (6.3%), although no PA was produced with Ru/H-ZSM-5 at the early stages of reaction. It should be noted here that much higher PA yields (45.8%) were previously obtained with the same Ru/H-ZSM-5 catalyst if dioxane is used as solvent. The lower yields obtained here with EHA thus indeed reflect the increasingly harsh conditions imposed by this solvent. Notably, the amount of Al lost to solution for Ru/H-β (10.6 $\mu g\,mL^{-1}$) was about three times the amount detected for Ru/H-ZSM-5 (4.0 $\mu g\,mL^{-1}$), as determined by AAS (Table S1). The extent and rate with which acid sites are lost during catalysis are considered to be responsible for the difference in activity.

To further determine the coordination of Al species and quantify the contribution of each in the zeolite-supported bifunctional catalysts, the 2D ^{27}Al 3QMAS and 1D ^{27}Al MAS NMR spectra of the fresh and spent Ru/H-ZSM-5 (ZSM-5-F and ZSM5-S-EHA) and Ru/H-β (β-F and β-S-EHA) catalyst materials were investigated. In Table 1, the peak parameters as determined by the EASY-GOING 2D fitting program and the relative intensities of the various Al peaks obtained from fitting the 1D NMR spectra are listed.

For the Ru/H-ZSM-5 samples (Figure 1 and Table 1), both zeolite ZSM5-F and ZSM5-S-EHA show two types of four-coordinated and two types of six-coordinated aluminum species and their relative intensities change during the catalytic reaction. For zeolite ZSM5-F, the Al^{IV}-M peak, which has an isotropic shift of around 54 ppm and a small C_Q of 1.36 MHz, represents tetrahedral framework aluminum (FAL);[45] The Al^{IV}-L resonance, with an isotropic shift of around 57 ppm and a C_Q of 5.96 MHz, shows increased horizontal broadening (evidenced from the F1 and F2 projection) with an unsymmetrical line shape, which is typically attributed to the influence of nearby cationic species. These cationic species could either originate from the hydrogenation metal (Ru) or from EFAL, with the latter being more likely.[32,46] Ru is unlikely to provide this charge compensation in the channels given its particle size (mean particle size ~4 nm) and low loading (1 wt%).[21] Moreover, aluminum spe-

Table 1. Fitted peak parameters and intensities for the solid-state NMR spectra of the two zeolite Ru/H-ZSM-5 and Ru/H-β samples under investigation, including their sample name used throughout the text.

Sample	Al type	$<C_Q>$ [MHz]	σ_Q [MHz]	δiso [ppm]	Δδ [ppm]	Fraction of spectral Intensity	Intensity normalized to ZSM5-F[a]
ZSM-5-F	Al^{IV}-L[b]	5.96	2.98	58.0	5.5	0.51	51
	Al^{IV}-M	1.36	0.68	54.9	4.3	0.32	32
	Al^{VI}-L	5.56	2.78	0.9	4.1	0.14	14
	Al^{VI}-M	1.60	0.80	0.0	2.4	0.04	4
ZSM-5-S-EHA	Al^{IV}-L	7.68	3.84	57.4	7.2	0.70	59
	Al^{IV}-M	2.34	1.17	53.9	5.2	0.19	16
	Al^{VI}-L	5.58	2.79	1.9	5.5	0.06	5
	Al^{VI}-M	2.28	1.14	0.5	5.0	0.05	4
β-F	Al^{IV}-L	5.80	2.90	59.0	7.5	0.32	32
	Al^{IV}-M	2.08	1.04	56.0	6.2	0.24	24
	Al^{IV}-S	1.02	0.51	53.9	2.2	0.08	8
	Al^{V}/(VI)	-	-	-	-	0.36	36
β-S-EHA	Al^{IV}-L	6.44	3.22	60.0	7.8	0.29	14
	Al^{IV}-M	3.72	1.86	56.7	4.6	0.33	17
	Al^{IV}-S	1.50	0.75	54.4	3.2	0.17	8
	Al^{V}/(VI)	-	-	-	-	0.21	10

[a] Based on 1D ^{27}Al MAS NMR fitting. The total Al signal of β-F has been normalized by weight and set to 100 g^{-1} of zeolite; the numbers give the individual contributions of these Al species to the total signal intensity; for ZSM-5-S-EHA and β-S-EHA the total signal intensity was normalized by weight, taking into account the coke content, and compared to the original signal intensity of the fresh sample. The other parameters are based on the ^{27}Al 3QMAS NMR spectra. [b] S: small C_Q; L: large C_Q; M: medium C_Q.

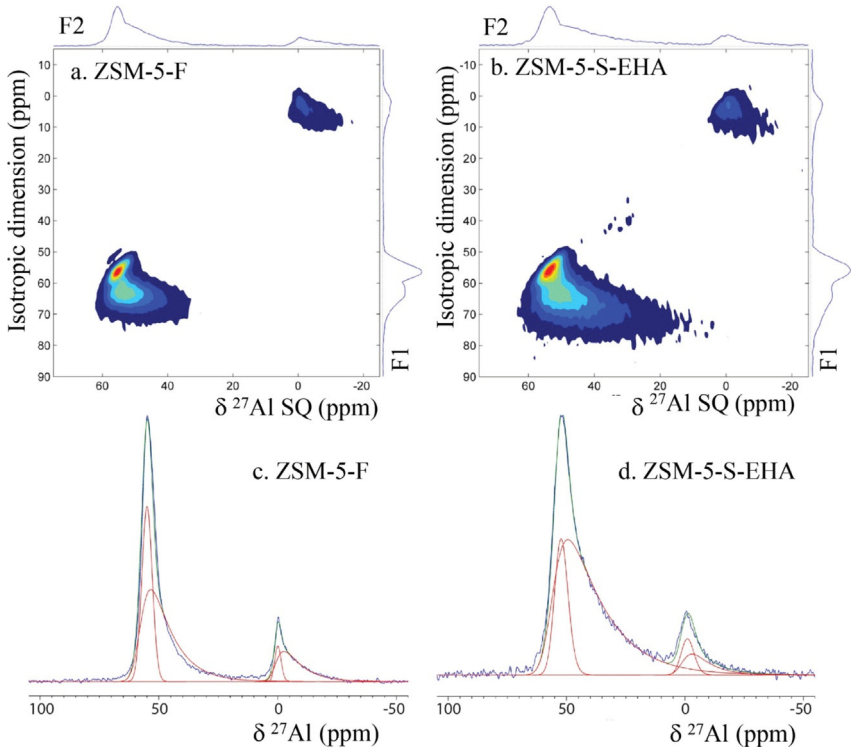

Figure 1. Top: ^{27}Al 3QMAS NMR spectra of: a) zeolite ZSM-5-F and b) zeolite ZSM-5-S-EHA. The 2D spectra are sheared so that the projection on the F1 axis gives an isotropic spectrum. Bottom: Normalized ^{27}Al MAS NMR spectra of: c) zeolite ZSM-5-F and d) zeolite ZSM-5-S-EHA (blue: experimental, green: fitted, red: simulated peaks).

cies interacting strongly with Ru ions would be difficult to observe, as the paramagnetic nature of these will enhance both T1 and T2 relaxation and make them become invisible, similar to previous reports on Fe-containing zeolites.[29] The distorted four-coordinated Al (Al^{IV}-L), most likely originate from tetrahedrally coordinated FAL that are compensated in their negative charge by EFAL that could have been formed during catalyst preparation.[28,33,47] In this respect, it seems more likely that the Al^{IV}-L signal is the result of EFAL species present in the MFI pores with coordination to FAL causing the distortion.[48–51]

Deng et al. also observed the broadened four-coordinated Al in ^{27}Al 3QMAS NMR of H-Y, and they assigned this distorted signal to EFAL species $Al(OH)^{2+}$.[50] The Al^{VI}-M species shows the standard parameters for six-coordinated extra-framework aluminum atoms (EFAl, δiso around 0 ppm and a small C_Q of 1.6 MHz) and can be assigned to octahedral EFAL $Al(OH)_3(H_2O)_3$; for the other octahedral Al^{VI}-L species with the larger C_Q of 5.56 MHz, distorted EFAL or three-coordinated FAL species with three additionally adsorbed water molecules have been suggested.[50]

Compared to zeolite ZSM5-F, the Al species in ZSM5-S-EHA show much broader line shapes in ^{27}Al 3QMAS NMR (Figure 1 b), as the EFAL in the pores are the cause of a short-range polarization effect, while an additional long-range geometrical effect is seen in ZSM5-S-EHA that gives rise to an increase in all the σ_Q and C_Q parameters.[39] The increase in all the parameters points at the increased heterogeneity of Al in ZSM5-S-EHA after catalysis. The relative contribution of each type Al species in each sample can be quantitatively obtained from the 1D ^{27}Al MAS NMR spectra (Figure 1 and Table 1). After catalysis, the amount of four-coordinated FAL (Al^{IV}-M, at $\approx$54 ppm with a symmetrical line shape) in Ru/H-ZSM-5 decreased from 32% to 16%; while that of distorted four-coordinated FAL (Al^{IV}-L, at $\approx$58 ppm with an unsymmetrical line shape) increased from 51% to 59%. This suggests the transition of FAL species to distorted FAL species, again thought to be the result of the coordination of dealuminated EFAL to FAL. The main change in Al speciation after catalysis is therefore the transition of four-coordinated, symmetric FAL (Al^{IV}-M) to distorted FAL (Al^{IV}-L), together with some minor dealumination, mainly of EFAL species.[35,48]

Figure 2 shows the ^{27}Al 3QMAS and ^{27}Al MAS NMR spectra for the Ru/H-β samples (β-F and β-S-EHA). In contrast to the H-ZSM-5 NMR data, it proved to be very challenging to fit the H-β spectra in the $Al^{V/(VI)}$ region; considering that the reaction is FAL-catalyzed, we therefore focused on the FAL region only for the β samples. Three types of four-coordinated Al species can be discerned in this case, the six-coordinated Al signal cannot be successfully fitted with the two resonances used previously (three signals should be used to fit the peak, but the resulting signal-to-noise ratio is too poor and line shapes are not well described). Furthermore, the five-coordinated Al species that are observed at around 30 ppm have too low an intensity to be fitted satisfactorily. The amounts of Al^{V} and Al^{VI} listed in the table were therefore obtained from the residual intensity left after fitting the tetrahedral Al. The ratio of four- to five-/six-coordinated Al again corresponds well to the one reported previously.[21] For β-F, the two sharp peaks of Al^{IV}-S (δiso = 53.9 ppm, C_Q = 1.02 MHz) and Al^{IV}-M (δiso = 56.0 ppm, C_Q = 2.08 MHz, slightly perturbed) represent symmetric tetrahedral FAL species; The Al^{IV}-L resonance (δiso = 59.0 ppm, C_Q = 5.8 MHz) is a highly perturbed FAL species, probably as a result of spatial proximity between four-coordinated FAL compensated in negative charge by EFAL cations.[49] Further evidence for this interaction can also be found in the FT-IR spectra after pyridine adsorption, as it would then be these EFAL that are responsible for the observed red shift in the LAS signal at 1446 cm^{-1} (see below). Five-coordinated EFAL can be clearly observed from the 1D fits of β-F, together with quite some six-coordinated EFAL species. Those species are generated via dealumination during the thermal treatment of the zeolites.[35,52]

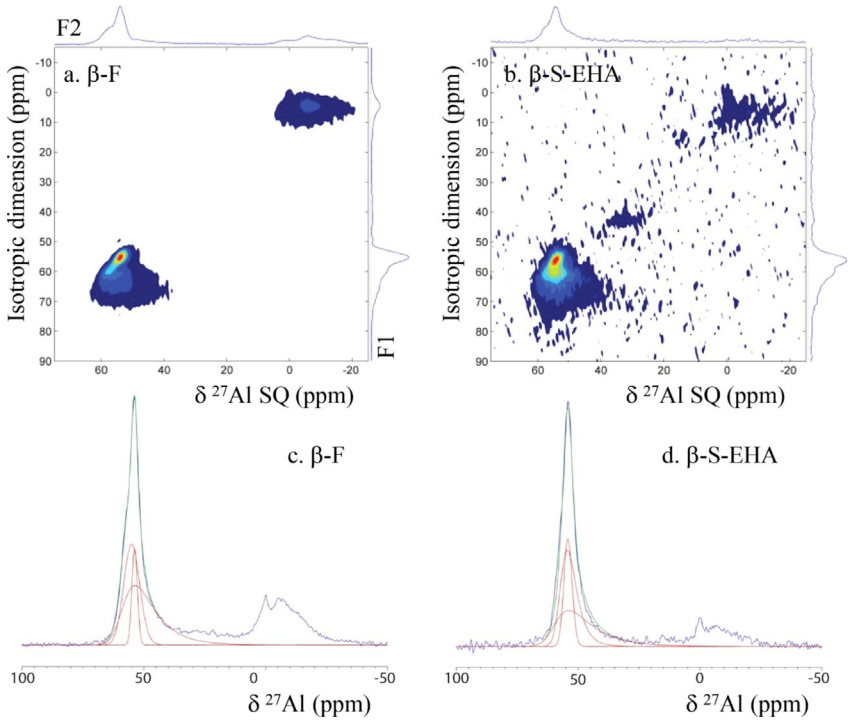

Figure 2. Top: ^{27}Al 3QMAS NMR spectra of: a) zeolite β-F, b) zeolite β-S-EHA. The 2D NMR spectra are sheared so that the projection on the F1 axis gives an isotropic spectrum. Bottom: normalized ^{27}Al MAS NMR spectra of: c) zeolite β-F, d) zeolite β-S-EHA (blue: experimental, green: fitted, red: simulated peaks).

For zeolite β-S-EHA, the intensity of all the four-coordinated FAL and six-coordinated EFAL species was found to have decreased significantly after catalysis (Figure 2). Compared to β-F, an overall loss of ~40% of all the four-coordinated FAL species was observed after the reaction in EHA. Of the different four-coordinated FAL species, a strong reduction in intensity was observed for Al^{IV}-M and Al^{IV}-L, but no loss of Al^{IV}-S was detected. Interestingly, analysis of the H-β catalyst after a reaction in neat LA instead of in EHA, showed that the Al^{IV}-S signal was reduced in intensity by half (Figure S2); this is surprising, given that conditions of the neat LA run are considered a lot milder than the EHA one; this might suggest that Al^{IV}-S can be approached by LA (minimum dimension of 3.3 Å), but not by EHA (minimum dimension of 5.3 Å), implying the Al^{IV}-S species to be located in the small channels of H-β. Finally, an overall loss of ~70% of all five-coordinated and six-coordinated EFAL species was observed for zeolite β-S-EHA. Clearly, much more extensive dealumination occurs for Ru/H-β than for Ru/H-ZSM-5 during reaction in EHA (Figure 3).

The changes seen in Al speciation by Al NMR and subsequent implications for catalyst stability are further corroborated by the FT-IR spectra of the fresh and spent zeolite-based samples. The hydroxyl stretching region of the FT-IR spectra as well as the FT-IR spectra obtained after pyridine adsorption (further denoted as Py-FT-IR) for the fresh and spent Ru/H-ZSM-5 catalysts are shown in Figure 4a,c. In the hydroxyl region, three main features can be seen, corresponding to hydroxyl groups assigned as BAS at 3602 cm^{-1}, as LAS at 3662 cm^{-1} and as terminal FAL silanol groups at 3735 cm^{-1}.[48,53,54] Only the BAS at 3602 cm^{-1} were found to decrease in intensity for zeolite ZSM-5-S-EHA, indicating some loss of these species during the catalytic reaction in EHA. Together with the NMR results, this decrease in BAS is considered

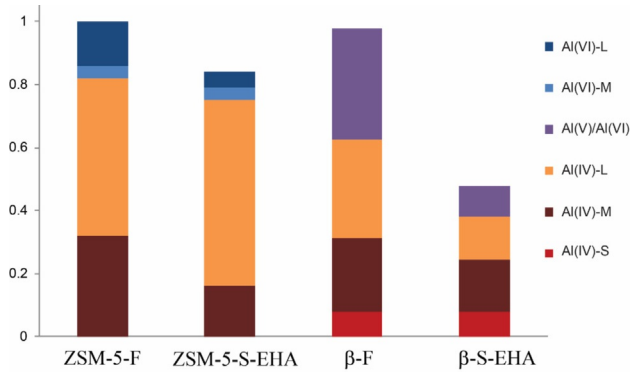

Figure 3. Relative amounts of four-, five-, and six-coordinated aluminum species in zeolites ZSM-5-F, ZSM-5-S-EHA, β-F and β-S-EHA, normalized to the total aluminum content in zeolite ZSM-5-F, as determined by ^{27}Al MAS NMR (accuracy ±2%).

the result of the reduction of FAL Al^{IV}-M species under reaction conditions. Only very minor changes were seen for the vibration at 3735 cm^{-1}, indicating little change in the number and type for the terminal FAL silanol groups. This is again in line with the NMR results, which showed only a minor change in total amount of FAL Al^{IV}-M and Al^{IV}-L species (Figure 3).

The Py-FT-IR spectra show a slight decrease in BAS, as evidenced by the small drop in intensity of the vibration at 1542 cm^{-1} for zeolite ZSM-5-S-EHA upon catalytic reaction in EHA. The vibration at 1454 cm^{-1} is instead assigned to the 19b ring vibration of pyridine interacting with EFAL species, for which again a slight decrease in intensity was observed after reaction. Notably, a new LAS feature at 1450 cm^{-1} was observed in zeolite ZSM-5-S-EHA, showing a red shift of 4 cm^{-1} compared to EFAL LAS sites. This shift should originate from pyridine molecules coordinated to EFAL as well as interacting

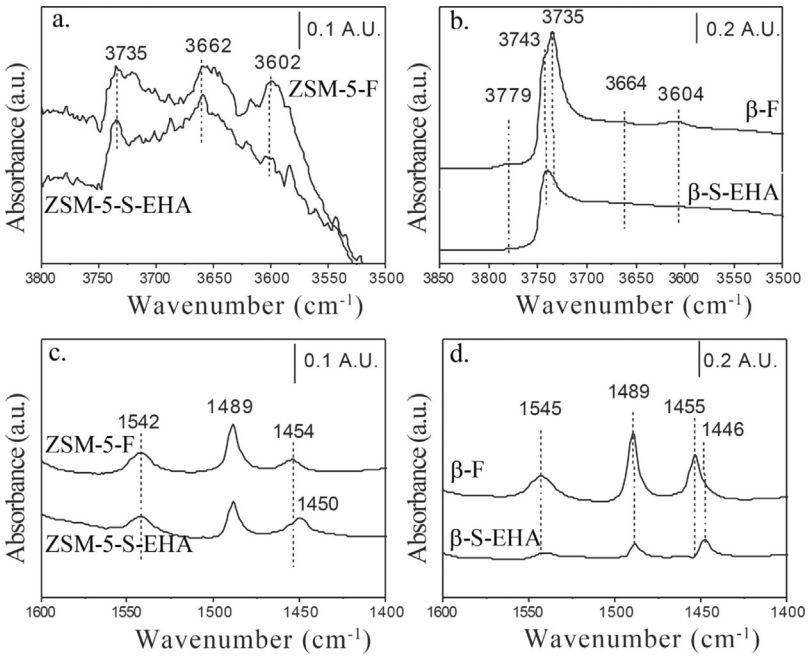

Figure 4. FT-IR spectra of the -OH stretching vibration region of the fresh and spent Ru/H-ZSM-5 (a) and Ru/H-β (b); vibrations assigned to BAS and LAS after pyridine adsorption of the fresh and spent Ru/H-ZSM-5 (c) and Ru/H-β (d) zeolite-based catalyst materials.[21]

with cationic species, such as Ru cation sites or a BAS proton.[55] The interaction of Ru-EFAL is very unlikely, given the relatively large Ru particles and the low loading, which would prevent this charge compensation in the channels; in addition, an observed increase in the intensity of 1450 cm^{-1} band for zeolite ZSM-5-S-EHA should lead to an increase in at least one EFAL species (Al^{VI}-M or Al^{VI}-L), which is not observed in the NMR results (Figure 3). Indeed, this vibration at 1450 cm^{-1} is more likely assigned to pyridine adsorbed on the EFAL species ending up being coordinated to FAL sites located in close proximity. In this respect, it seems more likely that the Al^{IV}-L signal is the result of EFAL species present in the MFI pores with coordination to FAL causing the distortion. Gener et al. also proposed these new LAS vibrations to originate from pyridine molecules that are both coordinated to a LAS as well as interacting through a hydrogen bond with protic site,[56] again implying that EFAL are actually in close proximity with FAL. The main change in Al speciation for zeolite Ru/H-ZSM-5 after catalysis is therefore the transition of four-coordinated, symmetric FAL (Al^{IV}-M) to FAL distorted by coordinated EFAL (Al^{IV}-L). Taken together with the slight decrease in BAS as seen in the Py-FT-IR spectra, this shows an increase in the disorder in strong acid sites in zeolite ZSM-5-S-EHA, as well as a small reduction in their number, upon catalysis. This limited loss of Al may be the result of the constraints imposed on the solvent or substrate by the small channel dimensions of zeolite H-ZSM-5, and the mutual attraction between highly charged EFAL and the negatively charged FAL prevents the EFAL from being washed out of the pores of H-ZSM-5.

For the Ru/H-β samples, five features can be seen in the hydroxyl region of the FT-IR spectra, associated with different -OH groups at 3604 cm^{-1} (FAL, BAS), 3664 cm^{-1} (LAS), 3735 cm^{-1} (terminal FAL silanol groups located at the internal surface), 3743 cm^{-1} (terminal EFAL silanol groups located at the external surface), and at 3779 cm^{-1} (LAS, -OH on small EFAL clusters, formed upon dealumination during calcination).[6,54,57–59] The decrease in intensity of the vibrations at 3604, 3664 and 3779 cm^{-1} for zeolite β-S-EHA demonstrates that both BAS and LAS sites have disappeared after reaction. A similar reduction in intensity of these particular features has also been reported as a result of acid leaching in previous studies.[54,57,60,61]

Compared to zeolite β-F, a sharp decrease in peak intensity at 3735 cm^{-1}, was observed for zeolite β-S-EHA. This suggests the reduction of the terminal FAL silanol groups in the catalyst material during reaction, for example, by leaching of FAL species together with a decrease in internal FAL silanol groups. Coalescence of the 3735 and 3743 cm^{-1} peaks was also seen for zeolite β-S-EHA, pointing to an increase in disorder of the zeolite structure. Similar results were also observed upon dealumination of zeolite H-β in oxalic acid at longer treatment time with condensation of adjacent silanol groups or silicon migration being proposed as possible reasons for this reduction in silanol groups.[8] Figure 4d show the FT-IR spectra of the fresh and spent Ru/H-β catalysts after pyridine adsorption. In zeolite β-S-EHA, the spent H-β samples showed a sharp decrease in intensity of the vibrations at 1455 cm^{-1}, 1490 cm^{-1} and 1545 cm^{-1}. This pronounced drop in pyridine-probed acid sites, suggests a considerable loss of both BAS and LAS for zeolite β-S-EHA. Interestingly, the red-shift LAS feature detected for zeolite ZSM-5-S-EHA, is again and now more clearly observed at 1446 cm^{-1} for the severely dealuminated β-S-EHA sample. The observed reduction in the number of silanol groups and the concomitant increase of this new type of LAS for zeolite β-S-EHA again imply that these new LAS could be EFAL species coordinated to BAS of FAL in close proximity in the spent catalyst materials, similar to those discussed above for zeolite ZSM-5-S-EHA. Indeed, Deng et al. previously proposed two possible structures for such sites in dealuminated HY in their study of the BAS/LAS synergy that has been observed for hydrocarbon reactions with these zeolites.[62] In conclusion, for zeolite H-β the severe loss of both BAS and LAS seen in the FT-IR spectra is in line with the leached Al detected in the liquid phase detected by AAS and the significant loss of FAL Al^{IV}-M, Al^{IV}-L and EFAL species observed by NMR, ultimately amounting to a nearly 40% loss of four-coordinated FAL species in the catalyst and a lower PA yield. Compared to zeolite Ru/H-ZSM-5, the higher degree of dealumination observed for zeolite Ru/H-β can be attributed to its larger channels, more flexible structure and the larger amount of crystal defects (i.e., more stacking faults) of zeolite H-β.[4,8,63]

The work presented here provides more detailed insight into the deactivation previously seen for Ru/H-ZSM-5 and Ru/H-β in the selective hydrogenation of LA into PA with EHA as solvent. Together, the NMR and FT-IR data now allow for deactivation to be related to leaching of Al and changes in the coordination of specific Al species, correlating well with prior observation that zeolite Ru/H-ZSM-5 is much more stable than zeolite Ru/H-β under these severe reaction conditions. This study thus provides direct insight into the overall stability and related changes in aluminum speciation and acidity of zeolite-based catalysts used for the valorization of biomass-derived molecules, highlighting the potential of these materials for future biomass conversion processes, but also the challenges faced under typical hydrothermal, liquid phase conversion conditions.

Acknowledgements

The authors gratefully thank the Smart Mix Program of the Netherlands Ministry of Economic Affairs and the Netherlands Ministry of Education, Culture and Science within the framework of the CatchBio Program. Support of NWO for the 'Solid-state NMR facility for Advanced Materials Science" is gratefully acknowledged.

Conflict of interest

The authors declare no conflict of interest.

Keywords: aluminum · hydrogenation · levulinic acid · nuclear magnetic resonance · zeolites

[1] A. Corma, *Chem. Rev.* **1995**, *95*, 559 – 614.
[2] Y. V. Kissin, *Catal. Rev. Sci. Eng.* **2001**, *43*, 85 – 146.
[3] E. Bourgeat-Lami, P. Massiani, F. Di Renzo, P. Espiau, F. Fajula, T. Des Courières, *Appl. Catal.* **1991**, *72*, 139 – 152.
[4] M. Müller, G. Harvey, R. Prins, *Microporous Mesoporous Mater.* **2000**, *34*, 135 – 147.
[5] E. G. Derouane, J. C. Védrine, R. R. Pinto, P. M. Borges, L. Costa, M. A. N. D. A. Lemos, F. Lemos, F. R. Ribeiro, *Catal. Rev. Sci. Eng.* **2013**, *55*, 454 – 515.
[6] M. Maache, A. Janin, J. C. Lavalley, J. F. Joly, E. Benazzi, *Zeolites* **1993**, *13*, 419 – 426.
[7] M. Guisnet, P. Ayrault, C. Coutanceau, M. F. Alvarez, J. Datka, *J. Chem. Soc. Faraday Trans.* **1997**, *93*, 1661 – 1665.
[8] M. R. Apelian, A. S. Fung, G. J. Kennedy, T. F. Degnan, *J. Phys. Chem.* **1996**, *100*, 16577 – 16583.
[9] D. Kubička, I. Kubičková, J. Čejka, *Catal. Rev. Sci. Eng.* **2013**, *55*, 1 – 78.
[10] P. A. Jacobs, M. Dusselier, B. F. Sels, *Angew. Chem. Int. Ed.* **2014**, *53*, 8621 – 8626; *Angew. Chem.* **2014**, *126*, 8765 – 8770.
[11] T. Ennaert, J. Van Aelst, J. Dijkmans, R. De Clercq, W. Schutyser, M. Dusselier, D. Verboekend, B. F. Sels, *Chem. Soc. Rev.* **2016**, *45*, 584 – 611.
[12] A. Fukuoka, P. L. Dhepe, *Angew. Chem. Int. Ed.* **2006**, *45*, 5161 – 5163; *Angew. Chem.* **2006**, *118*, 5285 – 5287.
[13] H. Wang, H. Ruan, M. Feng, Y. Qin, H. Job, L. Luo, C. Wang, M. H. Engelhard, E. Kuhn, X. Chen, M. P. Tucker, B. Yang, *ChemSusChem* **2017**, *10*, 1846 – 1856.
[14] W. Zhang, J. Chen, R. Liu, S. Wang, L. Chen, K. Li, *ACS Sustainable Chem. Eng.* **2014**, *2*, 683 – 691.
[15] D. W. Rackemann, W. O. S. Doherty, *Biofuels Bioprod. Biorefin.* **2011**, *5*, 198 – 214.
[16] J. J. Bozell, L. Moens, D. C. Elliott, Y. Wang, G. G. Neuenscwander, S. W. Fitzpatrick, R. J. Bilski, J. L. Jarnefeld, *Resour. Conserv. Recycl.* **2000**, *28*, 227 – 239.
[17] A. Corma, S. Iborra, A. Velty, *Chem. Rev.* **2007**, *107*, 2411 – 2502.
[18] W. R. H. Wright, R. Palkovits, *ChemSusChem* **2012**, *5*, 1657 – 1667.
[19] D. M. Alonso, S. G. Wettstein, J. A. Dumesic, *Green Chem.* **2013**, *15*, 584 – 595.
[20] J.-P. Lange, R. Price, P. M. Ayoub, J. Louis, L. Petrus, L. Clarke, H. Gosselink, *Angew. Chem. Int. Ed.* **2010**, *49*, 4479 – 4483; *Angew. Chem.* **2010**, *122*, 4581 – 4585.
[21] W. Luo, U. Deka, A. M. Beale, E. R. H. van Eck, P. C. A. Bruijnincx, B. M. Weckhuysen, *J. Catal.* **2013**, *301*, 175 – 186.
[22] W. Luo, P. C. A. Bruijnincx, B. M. Weckhuysen, *J. Catal.* **2014**, *320*, 33 – 41.
[23] A. M. Robinson, J. E. Hensley, J. W. Medlin, *ACS Catal.* **2016**, *6*, 5026 – 5043.
[24] A. Primo, H. Garcia, *Chem. Soc. Rev.* **2014**, *43*, 7548 – 7561.
[25] P. J. Van den Brink, K. L. Von Hebel, J.-P. Lange, L. Petrus, WO/2006/067171, **2006**.
[26] E. Lippmaa, A. Samoson, M. Magi, *J. Am. Chem. Soc.* **1986**, *108*, 1730 – 1735.
[27] L. S. de Saldarriaga, C. Saldarriaga, M. E. Davis, *J. Am. Chem. Soc.* **1987**, *109*, 2686 – 2691.
[28] D. Freude, H. Ernst, I. Wolf, *Solid State Nucl. Magn. Reson.* **1994**, *3*, 271 – 286.
[29] E. J. M. Hensen, Q. Zhu, R. A. J. Janssen, P. C. M. M. Magusin, P. J. Kooyman, R. A. van Santen, *J. Catal.* **2005**, *233*, 123 – 135.
[30] T.-H. Chen, B. H. Wouters, P. J. Grobet, *J. Phys. Chem. B* **1999**, *103*, 6179 – 6184.
[31] C. A. Fyfe, J. L. Bretherton, L. Y. Lam, *J. Am. Chem. Soc.* **2001**, *123*, 5285 – 5291.
[32] S. M. T. Almutairi, B. Mezari, G. A. Filonenko, P. C. M. M. Magusin, M. S. Rigutto, E. A. Pidko, E. J. M. Hensen, *ChemCatChem* **2013**, *5*, 452 – 466.
[33] E. R. H. van Eck, J. A. Z. Pieterse, A. P. M. Kentgens, *Solid State Nucl. Magn. Reson.* **2011**, *39*, 99 – 105.
[34] A. Omegna, M. Vasic, J. A. van Bokhoven, G. Pirngruber, R. Prins, *Phys. Chem. Chem. Phys.* **2004**, *6*, 447 – 452.
[35] J. Kanellopoulos, A. Unger, W. Schwieger, D. Freude, *J. Catal.* **2006**, *237*, 416 – 425.
[36] D. L. A. G. Grimminck, B. van Meerten, M. H. W. Verkuijlen, E. R. H. van Eck, W. L. Meerts, A. P. M. Kentgens, *J. Magn. Reson.* **2013**, *228*, 116 – 124.
[37] J. H. Baltisberger, Z. Xu, J. F. Stebbins, S. H. Wang, A. Pines, *J. Am. Chem. Soc.* **1996**, *118*, 7209 – 7214.
[38] A. Medek, J. S. Harwood, L. Frydman, *J. Am. Chem. Soc.* **1995**, *117*, 12779 – 12787.
[39] J. A. van Bokhoven, A. L. Roest, D. C. Koningsberger, J. T. Miller, G. H. Nachtegaal, A. P. M. Kentgens, *J. Phys. Chem. B* **2000**, *104*, 6743 – 6754.
[40] A. Abraham, S.-H. Lee, C.-H. Shin, S. B. Hong, R. Prins, J. A. van Bokhoven, *Phys. Chem. Chem. Phys.* **2004**, *6*, 3031 – 3036.
[41] J..-B. d'Espinose de Lacaillerie, C. Fretigny, D. Massiot, *J. Magn. Reson.* **2008**, *192*, 244 – 251.
[42] G. L. Caër, R. A. Brand, *J. Phys. Condens. Matter* **1998**, *10*, 10715.
[43] C. Gérard Le, B. Bruno, M. Dominique, *J. Phys. Condens. Matter* **2010**, *22*, 065402.
[44] G. Czjzek, J. Fink, F. Götz, H. Schmidt, J. M. D. Coey, J. P. Rebouillat, A. Liénard, *Phys. Rev. B* **1981**, *23*, 2513 – 2530.
[45] L. H. Ong, M. Dömök, R. Olindo, A. C. van Veen, J. A. Lercher, *Microporous Mesoporous Mater.* **2012**, *164*, 9 – 20.
[46] E. A. Pidko, S. M. T. Almutairi, B. Mezari, P. C. M. M. Magusin, E. J. M. Hensen, *ACS Catal.* **2013**, *3*, 1504 – 1517.
[47] D. L. Bhering, A. Ramírez-Solís, C. J. A. Mota, *J. Phys. Chem. B* **2003**, *107*, 4342 – 4347.
[48] S. Schallmoser, T. Ikuno, M. F. Wagenhofer, R. Kolvenbach, G. L. Haller, M. Sanchez-Sanchez, J. A. Lercher, *J. Catal.* **2014**, *316*, 93 – 102.
[49] S. Li, A. Zheng, Y. Su, H. Zhang, L. Chen, J. Yang, C. Ye, F. Deng, *J. Am. Chem. Soc.* **2007**, *129*, 11161 – 11171.
[50] Z. Yu, A. Zheng, Q. Wang, L. Chen, J. Xu, J.-P. Amoureux, F. Deng, *Angew. Chem. Int. Ed.* **2010**, *49*, 8657 – 8661; *Angew. Chem.* **2010**, *122*, 8839 – 8843.
[51] E. Brunner, H. Ernst, D. Freude, T. Fröhlich, M. Hunger, H. Pfeifer, *J. Catal.* **1991**, *127*, 34 – 41.
[52] S. M. Campbell, D. M. Bibby, J. M. Coddington, R. F. Howe, R. H. Meinhold, *J. Catal.* **1996**, *161*, 338 – 349.
[53] V. Bosáček, V. Patzelová, Z. Tvarůžková, D. Freude, U. Lohse, W. Schirmer, H. Stach, H. Thamm, *J. Catal.* **1980**, *61*, 435 – 442.
[54] A. Janin, M. Maache, J. C. Lavalley, J. F. Joly, F. Raatz, N. Szydlowski, *Zeolites* **1991**, *11*, 391 – 396.
[55] M. R. Mihályi, H. K. Beyer, *Chem. Commun.* **2001**, 2242 – 2243.
[56] J. P. Marques, I. Gener, P. Ayrault, J. C. Bordado, J. M. Lopes, F. R. Ribeiro, M. Guisnet, *Microporous Mesoporous Mater.* **2003**, *60*, 251 – 262.
[57] M. Trombetta, G. Busca, L. Storaro, M. Lenarda, M. Casagrande, A. Zambon, *Phys. Chem. Chem. Phys.* **2000**, *2*, 3529 – 3537.
[58] S. M. C. Menezes, V. L. Camorim, Y. L. Lam, R. A. S. San Gil, A. Bailly, J. P. Amoureux, *Appl. Catal. A* **2001**, *207*, 367 – 377.
[59] T. Armaroli, M. Bevilacqua, M. Trombetta, F. Milella, A. D. G. Alejandre, J. Ramírez, B. Notari, R. J. Willey, G. Busca, *Appl. Catal. A* **2001**, *216*, 59 – 71.
[60] S. Dzwigaj, M. Che, *J. Phys. Chem. B* **2006**, *110*, 12490 – 12493.
[61] E. B. Lami, F. Fajula, D. Anglerot, T. Des Courieres, *Microporous Mater.* **1993**, *1*, 237 – 245.
[62] S. Li, A. Zheng, Y. Su, H. Fang, W. Shen, Z. Yu, L. Chen, F. Deng, *Phys. Chem. Chem. Phys.* **2010**, *12*, 3895 – 3903.
[63] J. M. Newsam, M. M. J. Treacy, W. T. Koetsier, C. B. D. Gruyter, *Proc. R. Soc. London Ser. A* **1988**, *420*, 375 – 405.

Manuscript received: July 16, 2017
Revised manuscript received: September 30, 2017
Version of record online: November 22, 2017

